BIOCHEMISTRY
including biophysical chemistry & molecular biology

Article

pubs.acs.org/biochemistry

Insights into the Different Catalytic Activities of *Clostridium* Neurotoxins

Sheng Chen,*[,†] Andrew P. A. Karalewitz,[‡] and Joseph T. Barbieri[‡]

[†]Department of Applied Biology and Chemical Technology, The Hong Kong Polytechnic University, Hung Hom, Kowloon, Hong Kong SAR

[‡]Department of Microbiology and Molecular Genetics, Medical College of Wisconsin, Milwaukee, Wisconsin 53226, United States

Supporting Information

ABSTRACT: The clostridial neurotoxins are among the most potent protein toxins for humans and are responsible for botulism, a flaccid paralysis elicited by the botulinum toxins (BoNT), and spastic paralysis elicited by tetanus toxin (TeNT). Seven serotypes of botulinum neurotoxins (A–G) and tetanus toxin showed different toxicities and cleave their substrates with different efficiencies. However, the molecular basis of their different catalytic activities with respect to their substrates is not clear. BoNT/B light chain (LC/B) and TeNT light chain (LC/T) cleave vesicle-associated membrane protein 2 (VAMP2) at the same scissile bond but possess different catalytic activities and substrate requirements, which make them the best candidates for studying the mechanisms of their different catalytic activities. The recognition of five major P sites of VAMP2 (P7, P6, P1, P1′, and P2′) and fine alignment of sites P2 and P3 and sites P2 and P4 by LC/B and LC/T, respectively, contributed to their substrate recognition and catalysis. Significantly, we found that the S1 pocket mutation LC/T($K^{168}E$) increased the rate of native VAMP2 cleavage so that it approached the rate of LC/B, which explains the molecular basis for the lower k_{cat} that LC/T possesses for VAMP2 cleavage relative to that of LC/B. This analysis explains the molecular basis underlying the VAMP2 recognition and cleavage by LC/B and LC/T and provides insight that may extend the pharmacologic utility of these neurological reagents.

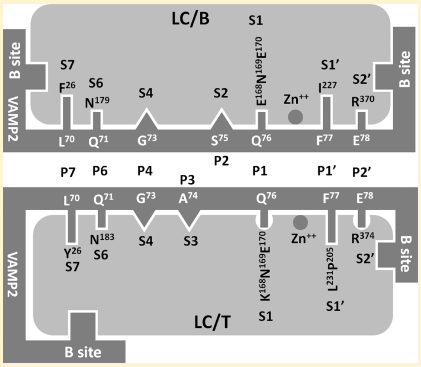

The clostridial neurotoxins (CNTs) are among the most potent protein toxins for humans and are responsible for botulism, a flaccid paralysis elicited by the botulinum toxins (BoNT), and spastic paralysis elicited by tetanus toxin (TeNT). CNTs are 150 kDa dichain proteins with typical A–B structure–function properties, where the B (binding) domain binds to surface components on the mammalian cell and translocates the A (active) domain to an intracellular location.[1] CNTs are organized into three functional domains: an N-terminal catalytic domain (light chain, LC), an internal translocation domain (heavy chain, HCT), and a C-terminal receptor binding domain (heavy chain, HCR).[2] The CNTs are zinc metalloproteases that cleave SNARE (soluble NSF attachment receptor) proteins, which interferes with the fusion of synaptic vesicles to the plasma membrane and ultimately blocks neurotransmitter release in nerve cells.[1,3] Mammalian neuronal exocytosis is driven by the formation of protein complexes between the vesicle SNARE protein, VAMP2, and the plasma membrane SNAREs, SNAP25 and syntaxin 1a.[4] There are seven BoNT serotypes (A–G) that cleave specific residues on one of three SNARE proteins: BoNT serotypes B, D, F, G, and TeNT cleave VAMP2, BoNT serotypes A and E cleave SNAP25, and BoNT serotype C cleaves SNAP25 and syntaxin 1a.[3,5−7]

BoNTs are considered as potential biological weapons and have been classified as a category A agent by the CDC (Center for Disease Control and Prevention, Atlanta, GA) in the United States.[6,7] To date, no effective treatment for BoNT intoxication has been developed, and the development of anti-botulism drugs is of upmost importance. An effective small molecular antitoxin is the most efficient way to treat human botulism, and the prerequisite for developing these inhibitors is to understand the molecular mechanism of the action of CNTs. In addition, BoNT/B has been approved by the Food and Drug Administration to treat cervical dystonia, while the relatively low activity of BoNT/B requires a higher dose of the toxin for effective treatment, which results in the development of immunoresistance in some patients.[8−10] An understanding of the mechanisms of substrate recognition of BoNT/B may help in the development of novel therapies with better pharmacological properties.

Unlike other zinc proteases, BoNTs and TeNT recognize an extended region of the SNARE proteins for substrate cleavage.[16−18] Recent studies using protein crystallography, protein modeling, and biochemical characterization of BoNTs revealed the mechanisms of substrate recognition by BoNT/A, BoNT/E, and BoNT/F.[11−14] While these three BoNTs recognize their substrates through important exosites and share a common theme, the substrate recognition is unique for

Received: January 3, 2012
Revised: March 29, 2012
Published: April 17, 2012

each of the BoNTs,[11,13,14] which requires that the mechanisms of substrate recognition and specificity be thoroughly investigated for each serotype. LC/B and LC/T cleave VAMP2, at the same scissile bond, but differ in catalytic activity, substrate requirement, and sensitivity to inhibitors.[12,15] Previous studies showed that LC/B and LC/T cleave VAMP2 with different K_m and k_{cat} values.[12,16] Alanine scanning mutagenesis and kinetic analysis identified three regions within VAMP2 that were recognized by LC/B and LC/T: residues adjacent to the site of scissile bond cleavage (cleavage region) and residues located within the N-terminal region and C-terminal region relative to the cleavage region.[12] Mutations at the P7, P4, P2, and P1′ residues of VAMP2 produced the greatest inhibition of LC/B cleavage (>32-fold), while mutations at P7, P4, P1′, and P2′ residues of VAMP2 produced the greatest inhibition of LC/T cleavage (>64-fold) [12] The different K_m values of LC/B and LC/T for VAMP2 may be attributed to the different compositions of binding sites to the N- and C-terminal sides of the LC active sites, while different k_{cat} values for VAMP2 may be due to different types of substrate recognition within the LC active site. This study addresses the molecular basis for the different types of recognition and cleavage of VAMP2 by LC/B and LC/T and may provide insights for the engineering of novel neurotoxin derivatives with improved therapeutic properties.

EXPERIMENTAL PROCEDURES

Plasmid Construction for Protein Expression. Plasmids for the expression of BoNT LC/B(1−430), LC/T(1−436), and VAMP2(1−97) and subsequent protein expression and purification were performed as previously described.[11,13,17] Site-directed mutagenesis of pLC/B, pLC/T, and pVAMP2 were performed using QuickChange (Stratagene) protocols as previously described.[11,13] Plasmids were sequenced to confirm the mutation and to confirm that additional mutations were not present within the ORFs. Mutated proteins were produced and purified as described above.[11−13,17]

Determination of Linear Velocities and Kinetic Constants for Cleavage of VAMP2 by LC/B and LC/T. Linear velocity reactions (10 μL) were performed as previously described.[11−13] VAMP2 proteins (5 μM) were incubated with varying concentrations of LC/B, LC/T, or LC derivatives in 10 mM Tris-HCl (pH 7.6) with 20 mM NaCl at 37 °C for 10 min. Reactions were stopped by adding sodium dodecyl sulfate−polyacrylamide gel electrophoresis (SDS−PAGE) buffer, and VAMP2 and the cleavage product were resolved by SDS−PAGE. The amount of VAMP2 cleaved was determined by densitometry. K_m and k_{cat} were determined with the same assay where VAMP2 concentrations were adjusted between 1 and 300 μM to achieve ∼10% cleavage by LC/B and LC/T. The reaction velocity versus substrate concentration was fit to the Michaelis−Menten equation, and kinetic constants were derived using GraphPad (San Diego, CA) Prism.

Compensatory Assay. The effect of compensatory mutations within LC/B and LC/T on the cleavage of VAMP2 and mutated forms of VAMP2 was assessed as previously described with modifications.[13] Briefly, 5 μM VAMP2 or VAMP2 derivatives were incubated with LC/B, LC/T, or LC derivatives at 37 °C for 20 min. The reactions were stopped via addition of SDS−PAGE sample buffer, and uncleaved and cleaved VAMP2 were resolved by SDS−PAGE. The amount of wild-type LC/B, LC/T, or LC derivative in the reaction mixture was plotted versus the percent cleavage, and the amount of LC required to cleave 50% of VAMP2 or the VAMP2 derivative was calculated.

Molecular Modeling. Structures of the LC/B−VAMP2 and LC/T−VAMP2 complexes were modeled using SWISS-MODEL and refined with PyMol (http://www.pymol.com) as described previously.[22] Protein Data Bank entries 1f82 for LC/B, 1z7h for LC/T, and 1xtg for the LC/A−SNAP25 complex were used in this analysis.

RESULTS

Molecular modeling was used to predict physical contacts between the LC/B−VAMP2 and LC/T−VAMP2 complexes to initiate the assessment of interactions that contribute to productive substrate cleavage (Figure 1 of the Supporting Information). Recognition of VAMP2 within the active pockets of LC/B and LC/T shared common contacts and also possessed unique associations that included a variation of the overall shape of the LC active site. Additional structure-based alignment of LC/B and LC/T showed that the amino acid composition of potential substrate recognition pockets differed at several of the pockets that contacted the VAMP2 residues that have been implicated in LC recognition. This may contribute to the different k_{cat} values of LC/B and LC/T for VAMP2. Biochemical approaches were used to define the different substrate recognition pockets so that the molecular basis of the differential catalytic activity of LC/B and LC/T could be addressed. Trypsin sensitivity analysis indicated that point mutations generated within LC/B and LC/T did not affect the rate of trypsin cleavage or the tryptic peptide generated, indicating that the overall conformations of the mutated LCs were similar to those of wild-type LCs (Figure 2 of the Supporting Information).

Recognition of VAMP2 by LC/B and LC/T. Modeling predicted the direct interactions for the S7, S6, S1, S1′, and S2′ substrate recognition pockets within the active sites of LC/B and LC/T with the respective P sites of VAMP2. This study focused on the characterization of the S7, S6, S1, S1′, and S2′ pockets within LC/B and LC/T along with the respective P sites of VAMP2.

S7 Pocket Recognition. In LC/B and LC/T, the S7 pocket comprised F^{26} and Y^{26}, respectively, which contacted L^{70}, the P7 residue of VAMP2 (Figure 1a). Cleavage of VAMP2($L^{70}A$) by LC/B and LC/T was ∼195- and ∼230-fold less efficient than cleavage of wild-type VAMP2, respectively (Table 1). The LC/B($F^{26}A$) and LC/T($Y^{26}A$) mutations produced an ∼5-fold increase in K_m and an ∼10-fold decrease in k_{cat} for VAMP2 cleavage (Table 2), while the mutation to Asp had a greater effect on kinetic values. The fact that the LC/B($F^{26}Y$) and LC/T($Y^{26}F$) mutations did not affect hydrolysis of VAMP2 indicated that L^{70} of VAMP2 and the aromatic S7 pocket residue of LC/B and LC/T interact through a similar hydrophobic interaction. Thus, although the physical interaction is unique to the analogous ionic S5−P5 contact between LC/A and SNAP25, the molecular outcomes of the S7−P7 interactions are similar, affecting both the affinity and rate of VAMP2 cleavage.[12]

S6 Pocket Recognition. In LC/B and LC/T, the S6 pocket comprised N^{179} and N^{183}, respectively, which contacted Q^{71}, the P6 residue of VAMP2 (Figure 1a). LC/B and LC/T cleaved VAMP2($Q^{71}A$) ∼15- and 6-fold slower (k_{cat}), respectively, than wild-type VAMP2 (Table 1). The $N^{1791}L$ and $N^{183}L$ mutations in LC/B and LC/T produced ∼4- and ∼2-fold reductions in k_{cat}, respectively, without affecting the K_m for VAMP2 cleavage (Table 2). The compensatory mutation sets, LC/B($N^{179}L$) and

dx.doi.org/10.1021/bi3000098 | Biochemistry 2012, 51, 3941−3947

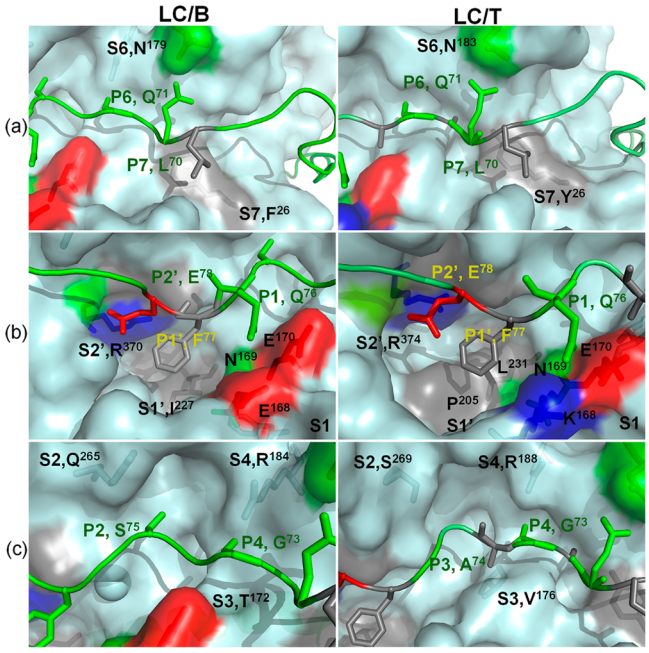

Figure 1. Recognition of VAMP2 P sites by LC/B and LC/T substrate recognition pockets. Computational and experimental data from this study provide a model for the interaction of LC/B (left) and LC/T (right) with VAMP2. (a) Recognition of P7 and P6 sites by S7 and S6 pockets of LC/B and LC/T. The S7 pocket of LC/B was formed by F^{26}, which recognized the P7 residue, L^{70}, and the S6 pocket of LC/B was formed by N^{179}, which recognized the P6 residue, Q^{71}. The S7 pocket of LC/T was formed by Y^{26}, which recognized the P7 residue, L^{70}, and the S6 pocket of LC/B was formed by N^{183}, which specifically recognized the P6 residue, Q^{71}. (b) Recognition of P1, P1′, and P2′ sites of VAMP2 by the S1, S1′, and S2′ pockets of LC/B and LC/T. The S1 pockets of LC/B and LC/T were formed by E^{168}, N^{169}, and E^{170} and by K^{168}, N^{169}, and E^{170}, respectively, and recognized the P1 residue of VAMP2, Q^{76}. The S1′ pockets of LC/B and LC/T were formed by I^{227} and by L^{231} and P^{205}, respectively, which recognized F^{77} of VAMP2. The S2′ sites of LC/B and LC/T were formed by R^{370} and R^{374}, respectively, which recognized the P2′ residue of VAMP2, E^{78}. (c) Fine alignment of P4, P3, and P2 sites of VAMP2 into the S4, S3, and S2 pockets of LC/B and LC/T. The large side chain of the S4 pocket residue, R, allows the alignment of the smaller side chain residue, G. The different shapes of S2 and S3 pockets of LC/B and LC/T, while not the residue composition of the pockets, allow S2 and S3 to tolerate different P2 and P3 site residues.

LC/T(N^{183}L), cleaved VAMP2(Q^{71}A) as efficiently as LC/B cleaved wild-type VAMP2 (Table 3). The positive correlation of the compensatory mutations supported a direct interaction (possibly via a hydrogen bond) between the S6 pocket N^{179} or N^{183} of the LCs and Q^{71} of VAMP2.

S1 Pocket Recognition. LC/B cleaved VAMP2(Q^{76}A) with a k_{cat} ~7-fold lower than that for cleavage of VAMP2 (Table 1). Mutations within the P1 site of VAMP2 (Q^{76}Y, Q^{76}F, Q^{76}R, and Q^{76}E) resulted in ~2-, ~6-, ~12-, and ~50-fold reductions in the k_{cat} of LC/B, respectively, without an effect on K_m, showing that hydrophobic residues were favored at this site and that the P1 pocket could accommodate an aromatic ring (Table 1). The S1 pocket of LC/B was formed by E^{168}, N^{169}, and E^{170} (Table 2 and Figure 1b). None of these residues showed a dominant interaction with P1 residue Q^{76} (Figure 1b), because the LC/B mutations E^{168}A, N^{169}A, and E^{170}A showed reductions in k_{cat} of ~20-, ~11-, and ~11-fold, respectively. The charge reversal mutation, LC/B(E^{170}K), had an ~130-fold

Table 1. Kinetic Constants of LC/B and LC/T with VAMP2 Point Mutations

		wild type	P7, L^{70} to A	P6, Q^{71} to A	P1, Q^{76} to A	P1, Q^{76} to Y	P1, Q^{76} to F	P1, Q^{76} to R	P1′, F^{77} to E	P2′, E^{78} to A	P2′, E^{78} to D	P2′, E^{78} to R	P2′, E^{78} to Y
LC/B	K_m (μM)	1.7 ± 0.3	6.5 ± 0.8	1.9 ± 0.2	1.8 ± 0.3	1.7 ± 0.3	1.8 ± 0.4	1.7 ± 0.4	1.8 ± 0.4	1.6 ± 0.2	2.4 ± 0.4	2.6 ± 0.2	2.2 ± 0.2	1.8 ± 0.2
	k_{cat} (min^{-1})	66.0	1.2	4.4	9.6	33.2	11.0	5.6	1.3	0.2	12.2	67.3	1.2	1.3
	k_{cat}/K_m (min^{-1} μM^{-1})	39.0	0.2	2.3	5.3	19.5	6.1	3.3	0.7	0.1	5.1	25.9	0.6	0.7
LC/T	K_m (μM)	4.1 ± 0.2	20.8 ± 0.8	4.1 ± 1.2	4.0 ± 0.6	4.1 ± 0.2	4.1 ± 0.3	4.0 ± 0.2	4.1 ± 0.6	3.8 ± 0.4	4.3 ± 0.4	4.1 ± 0.4	3.9 ± 0.3	N/D[a]
	k_{cat} (min^{-1})	9.6	0.1	1.6	1.3	9.4	9.4	1.5	1.9	0.02	0.05	9.7	0.2	N/D[a]
	k_{cat}/K_m (min^{-1} μM^{-1})	2.3	0.01	0.4	0.3	2.3	2.3	0.4	0.5	0.005	0.01	2.4	0.05	N/D[a]

[a]Not determined.

dx.doi.org/10.1021/bi3000098 | *Biochemistry* 2012, 51, 3941−3947

Table 2. Kinetic Constants of LC/B, LC/T, and LC Derivatives

	VAMP2 residue	LC pocket	LC derivative	K_m (μM)	k_{cat} (min^{-1})	k_{cat}/K_m (min^{-1} μM^{-1})
LC/B			wild-type LC/B	1.7 ± 0.3	66	39
	P7 (L^{70})	S7	$F^{26}A$	9.1 ± 0.8	5.6	0.6
			$F^{26}D$	35.6 ± 2.4	0.4	0.01
			$F^{26}Y$	1.8 ± 0.3	68	39
	P6 (Q^{71})	S6	$N^{179}L$	1.7 ± 0.4	16	9.4
	P1 (Q^{76})	S1	$E^{168}A$	1.7 ± 0.4	3.2	1.9
			$E^{168}K$	1.6 ± 0.2	0.4	0.3
			$N^{169}A$	1.8 ± 0.3	6.5	3.6
			$E^{170}A$	1.8 ± 0.4	6.6	3.7
	P1′ (F^{77})	S1′	$I^{227}A$	1.6 ± 0.2	0.8	0.5
			$I^{227}E$	1.8 ± 0.3	0.08	0.05
			$I^{227}L$	1.8 ± 0.4	0.1	0.07
	P2′ (E^{78})	S2′	$R^{370}A$	1.8 ± 0.4	0.6	0.4
			$R^{370}E$	1.8 ± 0.2	0.2	0.08
LC/T			wild-type LC/T	4.1 ± 0.2	9.6	2.3
	P7 (L^{70})	S7	$Y^{26}A$	20.8 ± 0.8	0.9	0.05
			$Y^{26}D$	N/D[a]	N/D[a]	N/D[a]
			$Y^{26}F$	4.2 ± 0.2	9.9	2.4
	P6 (Q^{71})	S6	$N^{183}L$	4.2 ± 0.4	4.5	1.1
	P1 (Q^{76})	S1	$K^{168}A$	4.2 ± 0.2	10.6	2.5
			$K^{168}E$	4.1 ± 0.2	79.8	19.5
			$N^{169}A$	4.0 ± 0.2	2.0	0.5
			$E^{170}A$	4.1 ± 0.6	2.6	0.63
	P1′ (F^{77})	S1′	$L^{231}A$	4.2 ± 0.2	0.3	0.8
			$L^{231}K$	N/D[a,b]	N/D[a]	N/D[a]
			$P^{205}A$	4.0 ± 0.3	0.3	0.8
			$P^{205}K$	N/D[a]	N/D[a]	N/D[a]
	P2′ (E^{78})	S2′	$R^{374}A$	N/D[a]	N/D[a]	N/D[a]
			$R^{374}E$	N/D[a]	N/D[a]	N/D[a]

[a]Not determined. [b]The mutant is too inactive to determine the kinetic constants.

Table 3. Results of a Compensatory Mutational Assay for Interactions of LC/B and LC/T with VAMP2

	50% cleavage of VAMP2 (nM)	ratio of activity (LC:LC derivative)	50% cleavage of VAMP2($Q^{71}A$) (nM)	ratio of activity (LC:LC derivative)
LC/B	6	4	96	1:16
LC/B($N^{179}L$)	24		6	
LC/T	120	2	720	1:6
LC/T($N^{183}L$)	240		120	
	50% cleavage of VAMP2 (nM)	ratio of activity (LC:LC derivative)	50% cleavage of VAMP2($G^{73}A$) (nM)	ratio of activity (LC:LC derivative)
LC/B	6	1	192	1:32
LC/B($R^{184}M$)	6		6	
LC/T	120	1	7680	1:64
LC/T($R^{188}M$)	20		60	
	50% cleavage of VAMP2 (nM)	ratio of activity (LC:LC derivative)	50% cleavage of VAMP2($E^{78}R$) (nM)	ratio of activity (LC:LC derivative)
LC/B	6	400	300	1:50
LC/B($R^{370}E$)	2400		6	
LC/T	120	300	>36000	N/D[a]
LC/T($R^{374}E$)	36000		>36000	

[a]Not determined.

slower k_{cat} (Table 2), suggesting that the negatively charged S1 pocket of LC/B favored recognition of the polar residue Q^{76}.

LC/T cleaved VAMP2($Q^{76}A$) ~8-fold slower than VAMP2 (Table 1). In contrast to LC/B, mutations at the P1 site of VAMP2 ($Q^{76}Y$, $Q^{76}F$, $Q^{76}R$, and $Q^{76}E$) showed no, no, ~6-fold, and ~5-fold reductions in the cleavage activity of LC/T, respectively, suggesting that the S1 pocket residues may interact with main chain components of VAMP2 (Table 1). The S1 pocket of LC/T was formed by K^{168}, N^{169}, and E^{170} (Figure 1b). Mutations $K^{168}A$, $N^{169}A$, and $E^{170}A$ in LC/T produced no, ~5-fold, and ~4-fold reductions in k_{cat}, respectively, while unexpectedly, LC/T($K^{168}E$) cleaved VAMP2 with an ~8-fold increased k_{cat}. The increased activity of LC/T($K^{168}E$) suggested that an acidic S1 pocket is optimal for Q^{76} recognition. Thus, the S1−P1 interaction may have structural and charge tolerance, implicating the S1 pocket of LC/T and LC/B as a candidate region for engineering and expanding the substrate potential to non-neuronal VAMP derivatives with therapeutic potential.

S1′ Pocket Recognition. In LC/B, S1′ pocket residue I^{227} contacted hydrophobic P1′ site residue F^{77} (Figure 1b). The VAMP2 P1′ mutation ($F^{77}A$) weakened by ~320-fold the ability of LC/B to hydrolyze (Table 1). LC/B($I^{227}A$) did not affect K_m but produced an ~80-fold reduction in k_{cat}, while LC/B($I^{227}E$) also did not affect K_m but produced an ~800-fold reduction in k_{cat} (Table 2). The mutation of other LC/B residues adjacent to I^{227}, including $F^{195}A$, $V^{200}A$, $L^{226}A$, and $S^{201}A$, did not affect LC/B cleavage of VAMP2 (data not

dx.doi.org/10.1021/bi3000098 | Biochemistry 2012, 51, 3941−3947

shown), supporting a direct interaction between I^{227} of LC/B and F^{77} of VAMP2. The conservative $I^{227}L$ mutation did not affect K_m but produced an ~550-fold reduction in k_{cat}, supporting the importance of the R group (side chain of the amino acid residue) orientation for optimal VAMP2 cleavage.

In LC/T, the S1′ pocket residues, L^{231} and P^{205}, contacted the hydrophobic P1′ site residue, F^{77} (Figure 1b). The VAMP2 P1′ mutation ($F^{77}A$) weakened by ~460-fold the ability of LC/T to hydrolyze VAMP2 (Table 1). The $L^{231}A$ or $P^{205}A$ mutation did not affect K_m but reduced the k_{cat} ~30-fold, while the $L^{231}K$ mutant became too inactive to determine its kinetic constants (Table 2). Mutation of other residues adjacent to S2 pocket residues L^{231} and P^{205}, including, $L^{232}A$, $F^{199}A$, $V^{204}A$, and $L^{230}A$, did not affect LC/T cleavage of VAMP2 (data not shown).

S2′ Pocket Recognition. LC/B cleaved the P2′ residue mutation VAMP2($E^{78}A$) slower than VAMP2 (Table 1). The $E^{78}R$ or $E^{78}Y$ mutation did not affect K_m but reduced k_{cat} ~50-fold, while the $E^{78}D$ mutation did not affect LC/B cleavage. This suggested that negatively charged residues were favored at the P2′ site (Table 1). In LC/B, S2′ pocket comprised R^{370} (Figure 1b). LC/B($R^{370}A$) cleaved VAMP2 with an ~100-fold lower k_{cat}, while LC/B($R^{370}E$) had an ~500-fold lower k_{cat} (Table 2). This was unexpected, because the corresponding Arg, R^{369}, within LC/A has been implicated in the transition state coordination of the P1 and P1′ site of SNAP25.[18] The direct contribution of R^{370} to P2′ site recognition was examined with compensatory mutation sets. This analysis showed that LC/B cleaved VAMP2($E^{78}R$) ~50-fold slower than VAMP2 and LC/B($R^{370}E$) cleaved VAMP2 ~400-fold slower than LC/B, while LC/B($R^{370}E$) has a rate of VAMP2($E^{78}R$) cleavage similar to the rate of VAMP2 cleavage by LC/B (Table 3). These data support a role for a salt bridge between R^{370} of LC/B and E^{78} of VAMP2, providing evidence of a direct interaction between P2′ residue E^{78} and the S2′ pocket residue, R^{370}, of LC/B.

LC/T cleaved VAMP2($E^{78}A$), a P2′ site mutation, ~230-fold slower that VAMP2 (Table 1). Like LC/B, LC/T had an ~50-fold lower k_{cat} for VAMP2($E^{78}R$), and the kinetic constants could not be determined for VAMP2($E^{78}Y$) because of the extremely low activity of LC/T on this VAMP mutation; the $E^{78}D$ mutation did not affect catalysis (Table 1). Also like that of LC/B, the S2′ pocket of LC/T contains an Arg, R^{374} (Figure 1b). LC/T($R^{374}A$) and LC/T($R^{374}E$) became too inactive for determination of their kinetic constants (Table 2). However, in contrast to LC/B, analysis of compensatory mutation sets showed that LC/T($R^{374}E$) did not cleave VAMP2($E^{78}R$) (Table 3). These data suggest that R^{374} of LC/T and E^{78} of VAMP2 do not directly interact or that the interaction is due to nonionic interactions between the two residues. This indicates a unique role for the S2′ pocket Arg of LC/B and LC/T that could be caused by positional differences within the respective S2′ pockets (Figure 1b).

VAMP2–LC Interactions at P Site Residues Not Predicted by Computational Predictions. While protein modeling predicted direct interactions between the S pocket residues of LC/B and LC/T and VAMP2, other LC S pockets, including S4, S3, and S2, were not predicted to have direct interactions with their respective R group of the P site residues. However, directed mutagenesis showed that G^{73} (P4) and S^{75} (P2) of VAMP2 were required for optimal LC/B cleavage and A^{72} (P5), G^{73} (P4), and A^{74} (P3) of VAMP2 were required for optimal LC/T cleavage.[12] Thus, while modeled LC/B–VAMP2 and LC/T–VAMP2 complexes did not predict direct R group interactions by these small R group amino acids ($A^{72}G^{73}A^{74}S^{75}$), these residues appear to facilitate alignment of VAMP2 with the active sites of LC/B and LC/T. Data support the former because the three-amino-acid-mutated VAMP2($A^{72}G$,$A^{74}G$,$S^{75}G$) was not cleaved by LC/B or LC/T (data not shown). Together, these data imply a role for the S4, S3, and S2 pockets in LC cleavage of VAMP2.

S4 Pocket. In LC/B, the S4 pocket that specifically recognized the P4 site of VAMP2, G^{73}, comprised one positively charged residue, R^{184} (Figure 1c). The LC/B $R^{184}M$ mutation that retained its positive charge, while with a smaller side chain, showed hydrolytic activity similar to that of wild-type LC/B (Table 3). However, LC/B($R^{184}M$) was able to cleave VAMP($G^{73}A$) as efficiently as wild-type LC/B was able to cleave wild-type VAMP2 (Table 3). These data suggested that the 32-fold decreased hydrolytic activity of LC/B on VAMP2($G^{73}A$) was due to the space constraint caused by adding a methyl group to P4 glycine and the replacement of R^{184} with a small side chain M complemented the larger side chain Ala at the P4 position.

In LC/T, the S4 pocket that specifically recognized the P4 site of VAMP2 G^{73} was formed by R^{188} (Figure 2). The

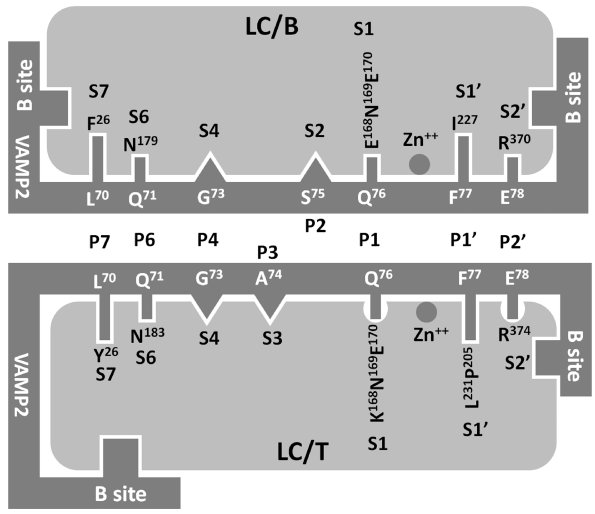

Figure 2. Similarities and differences in substrate recognition by LC/B and LC/T. The active site substrate recognition for LC/B includes the direct recognition of P7, P6, P1, P1′, and P2′ sites of VAMP2 by the corresponding S pockets in LC/B and the fine alignment of P4 and P3 sites with the S4 and S3 pockets, while the substrate recognition for LC/T includes the direct recognition of P7, P6, P1, P1′, and P2′ sites of VAMP2 by the corresponding S pockets in LC/T and the fine alignment of P4 and P2 sites with the S4 and S2 pockets. The less optimal composition of the S1 pocket and the more complex interaction between P2′ and S2′ in LC/T may contribute to the lower k_{cat} of LC/T on VAMP2.

LC/T $R^{188}M$ mutation with a smaller side chain, showed ~5-fold higher activity on VAMP2 than wild-type LC/T (Table 3). Furthermore, LC/T($R^{188}M$) was able to cleave VAMP $G^{73}A$ slightly more efficiently than wild-type LC/T was able to cleave wild-type VAMP2. These data also suggested that the 64-fold decreased hydrolytic activity of LC/T on VAMP2-($G^{73}A$) was due to the space constraint caused by the larger side chain residue Ala and the smaller side chain $R^{188}M$ mutation can complement the larger side chain Ala at the P4 position.

dx.doi.org/10.1021/bi3000098 | *Biochemistry* 2012, 51, 3941–3947

S3 Pocket Recognition. While LC/B cleaved VAMP2($A^{74}S$), a P3 mutation, as efficiently as VAMP2, LC/T cleaved VAMP2-($A^{74}S$) less efficiently than VAMP2.[12] The S3 pocket residues comprise T^{172} in LC/B and V^{176} in LC/T (Figure 1c). LC/B($T^{172}V$) and LC/T($V^{176}T$) cleaved VAMP2 as efficiently as the wild-type LCs (data not shown), suggesting the modifications in the polarity (-OH) at the S3 site were tolerated by both LCs. Structural comparison of S3 pockets indicated that the S3 pocket of LC/B was smaller than that of LC/T. This suggests that LC/T may be able to tolerate an increase in the size of P3 site residues, which may be coordinated by an adjacent β-sheet that is not conserved between LC/B and LC/T (Figure 1c).

S2 Pocket Recognition. While LC/T cleaved VAMP2-($S^{75}A$), a P2 mutation, as efficiently as VAMP2, LC/B cleaved VAMP2($S^{75}A$) less efficiently than VAMP2.[12] The S2 pocket was formed by Q^{265} in LC/B and S^{269} in LC/T (Figure 1c). LC/B($Q^{265}S$) and LC/T($S^{269}Q$) were as efficient as wild-type LCs for VAMP2 cleavage (data not shown). This suggests that the differential efficiency of LC/B and LC/T cleavage of VAMP2($A^{74}S$) was not due to the composition of the corresponding substrate recognition pockets. Comparison of S2 pockets of LC/B and LC/T showed that the S2 pocket of LC/B was wider than that of LC/T, which could allow LC/B to tolerate the addition of the -OH group of Ser (Figure 1c).

DISCUSSION

Earlier studies showed that LC/B and LC/T recognized three regions in VAMP2 that contribute to substrate recognition: a cleavage region (residues 70−78) that immediately surrounds the scissile bond and two regions that contribute to high-affinity binding to VAMP2 that are located N-terminal and C-terminal to the cleavage region.[12,16] Together with this study, the generation of a detailed model for how LC/B and LC/T recognize VAMP2 and a molecular basis for explaining the similarities and differences in substrate cleavage are now possible. By analogy with LC/A−SNAP25 interactions,[13,19] upon N-terminal and C-terminal VAMP2 binding, the S7 pocket residue (F^{26} in LC/B and Y^{26} in LC/T) associates with L^{70} in the P7 site through hydrophobic interactions and the S2′ pocket residue (R^{370} in LC/B and R^{374} in LC/T) associates through an ionic interaction with E^{78}, the P2′ residue. These interactions facilitate association of P1 and P1′ (Q^{76} and F^{77}, respectively) with the LCs to align the scissile bond for substrate cleavage. In addition, interactions of the internal S pocket residues of LC/B and LC/T (S5, S4, S3, and S2) align VAMP2 through physical interactions that allow physical orientations for the effective cleavage of a coiled substrate.

The similarity of LC/B and LC/T substrate recognition includes two binding sites that are unique in *Clostridium* neurotoxins and the specific recognition of several P sites by active site pockets of the LCs, where the P7−S7 and P1′−S1′ interactions are the most important anchoring points, while other P−S interactions contribute to the tighter and more specific substrate recognition. The different substrate recognition between these two neurotoxins includes their different binding sites that may contribute to their different K_m values on substrate VAMP2 and the different compositions of their S pockets, which may contribute to their different k_{cat} values on VAMP2. The active site substrate recognition for LC/B includes the direct recognition of P7, P6, P1, P1′, and P2′ sites of VAMP2 by the corresponding S pockets in LC/B and the fine alignment of P4 and P3 sites with the S4 and S3 pockets, while the substrate recognition for LC/T includes the direct recognition of P7, P6, P1, P1′, and P2′ sites of VAMP2 by the corresponding S pockets in LC/T and the fine alignment of P4 and P2 sites with the S4 and S2 pockets. The less optimal composition of the S1 pocket and the more complex interaction between P2′ and S2′ in LC/T may contribute to the lower k_{cat} of LC/T on VAMP2 (Figure 2).

The residues within the cleavage regions vary among the BoNT serotypes. In a comparison of the cleavage regions that are recognized by the LCs, the P2′ and P2 sites of LC/E and LC/F, the P4′ and P5 sites of LC/A, and the P2′ and P7 sites of LC/B and LC/T contribute to P1′−P1 scissile bond stabilization. The different arrangements of P sites that are recognized by LCs to stabilize the scissile bond correlate with LC catalytic potential. LC/E and LC/F have high k_{cat} values and compact cleavage regions, while LC/B and LC/T have low k_{cat} values and extended cleavage regions. The larger cleavage region may result in weak stabilization of scissile bond cleavage.[11−13,16,19,20]

Relative to LC/B, the low k_{cat} for LC/T appears to be attributed to less than optimal interactions between the P1 residue and the S1 pocket residues and possibly between the P2′ residue and the S2′ pocket. The observation that the introduction of an ionic bond between the P1 residue and the S1 pocket residue enhances the k_{cat} provided a basis for the lower k_{cat} of LC/T relative to that of LC/B. This suggests that the fastest rate of substrate cleavage may not be optimal in a biological setting. This also indicates that there is the potential for additional optimization to modulate BoNTs with higher activity, which may be a potential solution to the immune resistance issue of BoNT-based therapies.

Although the precise mechanism for peptide bond cleavage by the BoNTs remains to be resolved, cleavage of the scissile peptide bond appears to follow a general base-catalyzed mechanism.[18,21,22] Arg^{362} and Tyr^{365} interact with the carbonyl oxygen of the P1 and P1′ residues of SNAP25, respectively, with stabilization of the oxyanion in the transition state. Peptide bond cleavage is initiated by a water molecule that is polarized by the Glu within the zinc binding motif (HEXXH) and Zn^{2+}, which causes a nucleophilic attack on the carbonyl carbon of the scissile bond to form an oxyanion. Peptide bond cleavage is likely achieved by the transfer of a proton from the attacking water mediated by the carboxyl group of the downstream Glu to form a protonated amine. The crystal structure of LC/E bound to the C-terminus of the LC/E-cleaved SNAP25 product showed that the P1′ oxygen interacts with the side chain NH1 and NH2 groups of the conserved residue Arg^{347} and the OH group of Tyr^{350} interacts with the P2′ Met^{182} oxygen and helps in stabilizing its main chain, which confirms that Arg^{347} and Tyr^{350} play a crucial role in transition state stabilization by allowing proper docking of the main chain of P1, P1′, and P2′ residues at the active site. Our study shows a different (additional) role for R^{370} of LC/B. Complementation assays indicated that R^{370} of LC/B is directly involved in substrate recognition and specifically recognized the P2 residue, E^{78}, of VAMP2. In contrast, although the S2′ pockets in LC/B and LC/T were very similar, R^{368} of LC/T and the P2 residue, E^{78}, did not show direct interaction. The role of R^{374} in LC/T is not clear; it may be involved in the coordination of substrate catalysis. The role of this analogous Arg in other serotypes of BoNTs will need to be determined for further confirmation.

In conclusion, the comparative characterization addressed the molecular mechanisms of VAMP2 recognition and cleavage by LC/B and LC/T and described the molecular basis of their

similarities and differences. The novel information regarding BoNT substrate recognition presented may facilitate the engineering of novel BoNTs to extend BoNT-based therapies.

■ ASSOCIATED CONTENT

Supporting Information

Recognition of VAMP2 P site residues within the active site regions of LC/B and LC/T (Figure 1) and trypsin digestion profiles of LC/B, LC/T, and their derivatives (Figure 2). This material is available free of charge via the Internet at http://pubs.acs.org.

■ AUTHOR INFORMATION

Corresponding Author

*Telephone: (852)-3400-8795. Fax: (852)-2364-9932. E-mail: bcschen@polyu.edu.hk.

Funding

This work was sponsored by RGC/Hong Kong PolyU Competitive Research Grants A-PK05 and G-YJ15 to S.C. and Great Lakes Regional Center of Excellence Grant U54 AI057153 for J.T.B.

Notes

The authors declare no competing financial interest.

■ ACKNOWLEDGMENTS

We thank the members of S.C.'s laboratory for helpful discussion.

■ ABBREVIATIONS

BoNT/B, botulinum neurotoxin serotype B; TeNT, tetanus neurotoxin; LC, light chain; VAMP2, vesicle-associated membrane protein 2; SNARE, soluble NSF attachment receptor.

■ REFERENCES

(1) Montecucco, C., and Schiavo, G. (1994) Mechanism of action of tetanus and botulinum neurotoxins. *Mol. Microbiol. 13*, 1−8.

(2) Davletov, B., Bajohrs, M., and Binz, T. (2005) Beyond BOTOX: Advantages and limitations of individual botulinum neurotoxins. *Trends Neurosci. 28*, 446−452.

(3) Montecucco, C., and Schiavo, G. (1993) Tetanus and botulism neurotoxins: A new group of zinc proteases. *Trends Biochem. Sci. 18*, 324−327.

(4) Brunger, A. T. (2005) Structure and function of SNARE and SNARE-interacting proteins. *Q. Rev. Biophys. 38*, 1−47.

(5) Schiavo, G., Benfenati, F., Poulain, B., Rossetto, O., Polverino de Laureto, P., DasGupta, B. R., and Montecucco, C. (1992) Tetanus and botulinum-B neurotoxins block neurotransmitter release by proteolytic cleavage of synaptobrevin. *Nature 359*, 832−835.

(6) Schiavo, G., Malizio, C., Trimble, W. S., Polverino de Laureto, P., Milan, G., Sugiyama, H., Johnson, E. A., and Montecucco, C. (1994) Botulinum G neurotoxin cleaves VAMP/synaptobrevin at a single Ala-Ala peptide bond. *J. Biol. Chem. 269*, 20213−20216.

(7) Schiavo, G., Rossetto, O., Benfenati, F., Poulain, B., and Montecucco, C. (1994) Tetanus and botulinum neurotoxins are zinc proteases specific for components of the neuroexocytosis apparatus. *Ann. N.Y. Acad. Sci. 710*, 65−75.

(8) Brashear, A., Lew, M. F., Dykstra, D. D., Comella, C. L., Factor, S. A., Rodnitzky, R. L., Trosch, R., Singer, C., Brin, M. F., Murray, J. J., Wallace, J. D., Willmer-Hulme, A., and Koller, M. (1999) Safety and efficacy of NeuroBloc (botulinum toxin type B) in type A-responsive cervical dystonia. *Neurology 53*, 1439−1446.

(9) Atassi, M. Z., Jankovic, J., Steward, L. E., Aoki, K. R., and Dolimbek, B. Z. (2012) Molecular immune recognition of botulinum neurotoxin B. The light chain regions that bind human blocking antibodies from toxin-treated cervical dystonia patients. Antigenic structure of the entire BoNT/B molecule. *Immunobiology 217*, 17−27.

(10) Atassi, M. Z., Dolimbek, B. Z., Jankovic, J., Steward, L. E., and Aoki, K. R. (2008) Molecular recognition of botulinum neurotoxin B heavy chain by human antibodies from cervical dystonia patients that develop immunoresistance to toxin treatment. *Mol. Immunol. 45*, 3878−3888.

(11) Chen, S., and Barbieri, J. T. (2007) Multiple pocket recognition of SNAP25 by botulinum neurotoxin serotype E. *J. Biol. Chem. 282*, 25540−25547.

(12) Chen, S., Hall, C., and Barbieri, J. T. (2008) Substrate recognition of VAMP-2 by botulinum neurotoxin B and tetanus neurotoxin. *J. Biol. Chem. 283*, 21153−21159.

(13) Chen, S., Kim, J. J., and Barbieri, J. T. (2007) Mechanism of substrate recognition by botulinum neurotoxin serotype A. *J. Biol. Chem. 282*, 9621−9627.

(14) Chen, S., and Wan, H. Y. (2011) Molecular mechanisms of substrate recognition and specificity of botulinum neurotoxin serotype F. *Biochem. J. 433*, 277−284.

(15) Foran, P., Shone, C. C., and Dolly, J. O. (1994) Differences in the protease activities of tetanus and botulinum B toxins revealed by the cleavage of vesicle-associated membrane protein and various sized fragments. *Biochemistry 33*, 15365−15374.

(16) Sikorra, S., Henke, T., Galli, T., and Binz, T. (2008) Substrate recognition mechanism of VAMP/synaptobrevin-cleaving clostridial neurotoxins. *J. Biol. Chem. 283*, 21145−21152.

(17) Chen, S., and Wan, H. Y. (2011) Molecular mechanisms of substrate recognition and specificity of botulinum neurotoxin serotype F. *Biochem. J. 433*, 277−284.

(18) Binz, T., Bade, S., Rummel, A., Kollewe, A., and Alves, J. (2002) Arg(362) and Tyr(365) of the botulinum neurotoxin type a light chain are involved in transition state stabilization. *Biochemistry 41*, 1717−1723.

(19) Chen, S., and Barbieri, J. T. (2006) Unique substrate recognition by botulinum neurotoxins serotypes A and E. *J. Biol. Chem. 281*, 10906−10911.

(20) Sikorra, S., Henke, T., Swaminathan, S., Galli, T., and Binz, T. (2006) Identification of the amino acid residues rendering TI-VAMP insensitive toward botulinum neurotoxin B. *J. Mol. Biol. 357*, 574−582.

(21) Agarwal, R., Schmidt, J. J., Stafford, R. G., and Swaminathan, S. (2009) Mode of VAMP substrate recognition and inhibition of *Clostridium botulinum* neurotoxin F. *Nat. Struct. Mol. Biol. 16*, 789−794.

(22) Agarwal, R., Eswaramoorthy, S., Kumaran, D., Binz, T., and Swaminathan, S. (2004) Structural analysis of botulinum neurotoxin type E catalytic domain and its mutant Glu212→Gln reveals the pivotal role of the Glu212 carboxylate in the catalytic pathway. *Biochemistry 43*, 6637−6644.